Density functional study of layering at liquid surfaces

R. Checa,[1] E. Chacón,[2] and P. Tarazona[1,3]
[1]*Departamento de Física Teórica de la Materia Condensada (C-V), Universidad Autónoma de Madrid, E-28049 Madrid, Spain*
[2]*Instituto de Ciencia de Materiales de Madrid, CSIC, E-28049 Madrid, Spain*
[3]*Instituto Nicolás Cabrera, Universidad Autónoma de Madrid, E-28049 Madrid, Spain*
(Received 23 July 2004; published 7 December 2004)

We analyze the density profiles for liquid-vapor interfaces within two density functional (DF) approximations, applied to simple fluid models which have low ratios between their triple and critical temperatures. The observation of layering structures at low T is discussed in relation with the Fisher-Widom line for each model. Although we find no apparent correlation between the amplitude of the oscillatory density decay mode and the approach to T_{FW}, that temperature sets a threshold for the generation of nonmonotonic structures within a fixed distance of the interface. The rapid decay of the oscillatory mode amplitude with T may be interpreted as a result of the capillary wave (CW) damping of strongly structured intrinsic density profiles. The layering in the presence of gravitylike external fields indicate that the effective transverse size which might be built in the DF approximations is around 10 ± 2 molecular diameters; however, that interpretation has to allow for an effectively reduced damping exponent, i.e., an effective surface tension for the CW Hamiltonian which is larger than the value obtained directly from the DF grand-potential minimization.

DOI: 10.1103/PhysRevE.70.061601 PACS number(s): 68.03.Kn, 61.20.Gy

I. INTRODUCTION

Accurate nonlocal density functional (DF) approximations [1] have been developed, over the last decades, to describe the strong layering structures in the density profiles of wall-fluid interfaces. The same DF approximations have been used to describe liquid-vapor interfaces, generally in good agreement with the results of the simplest square-gradient approximation [2], which describes the free liquid surface as a smooth monotonic density profile $\rho(z)$. Some early theoretical predictions [3] of layered structures at the free surface of the Lennard-Jones (LJ) liquid, near its triple point temperature T_t, were apparently supported by computer simulation results [4], but not confirmed by improved theoretical treatments, nor by computer simulations with larger system sizes and equilibration times, so that the presence of molecular layering at free liquid surfaces was disregarded during two decades. In the last few years, there has been a revival of the subject, based on new evidence from experiments [5], theory [6], and computer simulations [7]. The increasing accuracy of the experimental results for the x-ray reflectivity on liquid surfaces has given clear evidence of atomic layering for some liquid metals, Hg [8], Ga [9], and more recently for alkali-metal mixtures [10]. In parallel, a generic DF analysis [6] has predicted the common exponential decay modes $\rho(z)-\rho_o \sim \exp(-\zeta z)$ towards a bulk density ρ_o. The decay constants ζ are determined by the direct correlation function of the bulk fluid, so that they should be common to the density profiles of the free liquid surface, to the interfaces of the same liquid against solid walls, and to the radial distribution function $g(r)$. The complex values $\zeta_c = \alpha \pm iq$ represent decaying layered structures, while the real values $\zeta_r = \beta$ give monotonically decaying density profiles (we assume $\alpha,\beta > 0$ with the bulk phase filling the $z \geqslant 0$ semispace). The asymptotic behavior of $\rho(z)$ towards the bulk phase would be controlled by the slowest decay mode, i.e., that with the lowest real part for ζ. The Fisher-Widom (FW) line, on the (ρ_o, T) plane, was originally defined [11] in terms of the asymptotic decay of $g(r)$ in a liquid, and it was later recognized [6] as the generic boundary between the liquid states with an asymptotic oscillatory decay ($\alpha < \beta$) and those with a monotonic exponential decay ($\alpha > \beta$). Other (real or complex) roots with larger real part are not relevant for the discussion, so that we refer to $\zeta_c = \alpha \pm iq$ and $\zeta_r = \beta$ as the two roots with the lowest real parts. The imaginary component q of the complex root ζ_c is always found to be around $2\pi/\sigma$, as it corresponds to the formation of molecular layers in $\rho(z)$, with period similar to the molecular diameter σ.

The estimations for LJ and other simple-fluid models [12] locate most of the liquid coexisting phase on the oscillatory side of the FW line, which intercepts the liquid-vapor coexistence at temperatures T_{FW} of only about 10% below the critical temperature T_c. Oscillating tails in $\rho(z)$ were found in some DF calculations, although their amplitude (which cannot be predicted from the linear DF analysis) was found to be very small. In practice, the accurate fit of the density profile tails often requires adding an oscillatory and a monotonic decaying mode,

$$\rho(z) - \rho_o = A\, e^{-(\alpha \pm iq)z} + B\, e^{-\beta z} + \cdots. \tag{1}$$

The same liquid bulk has very different values for A and B at the vapor-liquid, at wall-liquid interfaces, or around an identical test particle used to get the radial distribution function $g(r) = \rho(r)/\rho_o$. Thus, the qualitative aspect of the liquid-vapor $\rho(z)$ may be very different from that of a wall-fluid interface, or from $g(r)$, and only the truly asymptotic behavior would be common. The strong oscillations of $g(r)$, typically observed even at $T > T_{FW}$, contrast with the empirical evidence of monotonic decays for the liquid-vapor and liquid-liquid density profiles in DF approximations unless T is well below T_{FW} [6,14]. The logic behind such behavior could be based

on the difference between *external* boundary conditions like those imposed by a wall-fluid potential energy [or the equivalent spherical potential imposed by the test-particle representation of $g(r)$], and the *free surface* of a liquid at the interface produced by its own molecular interactions. However, there is no theoretical proof of such conjecture, which escapes from the linear DF perturbation analysis used to identify the exponential decays $\zeta_c = \alpha \pm iq$ and $\zeta_r = \beta$.

The experimental evidence of atomic layering at the free surfaces of liquid Hg [8] and Ga [9] was first supposed to be a consequence of the metallic character of these liquids, with the electrons providing an effective external potential for the ions. However, an alternative interpretation of that theoretical evidence was given through the development, and Monte Carlo (MC) simulations, of simple models with pairwise interactions [7,16,17], devised to have low melting temperatures, with ratios T_t/T_c between the triple and critical temperatures similar to the experimental values of Hg and Ga. Strong layering structures were observed in the MC density profiles for these models at $T/T_c < 0.2$, far below the range of the stable liquid phase of the LJ or other simple fluid models. Moreover, models representing different mechanisms to get low T_t/T_c ratio may have very different FW lines but still give similar amplitudes for the oscillatory decay mode $A(T)$, decaying as T/T_c increases, but without apparent correlation with the value of T_{FW} for each model. The first objective of this paper is to explore the connection between the layering at free liquid surfaces and the FW line, within DF approximations for the same *cold liquid* models explored in MC simulations.

Our second objective is the connection between the capillary wave (CW) theory [2,18] and the liquid-vapor density profiles given by DF approximations. The CW surface fluctuations are assumed to produce local shifts of an *intrinsic profile*, so that the interfacial width of the liquid-vapor density profile would depend on the sampled transverse area L^2, through the low-wavelength cutoff in the CW spectrum. The L dependence of $\rho(z,L)$ is very weak (logarithmic) for monotonic profiles [19], but for oscillatory profiles it becomes powerlike, with $A(L) \sim L^{-\eta(T)}$ for the amplitude of the oscillations [20]. The exponent

$$\eta(T) = \frac{kT(\alpha^2 + q^2)}{4\pi\gamma} \approx \frac{kT\pi}{\gamma\sigma^2} \tag{2}$$

depends on the temperature, on the modulus of the complex decay constant $\zeta_c = \alpha \pm iq$, and on the surface tension γ [15]. The dimensionless function $\eta(T/T_c)$ takes very similar values for different models of the molecular interactions [16], increasing with the temperature. The typical simple liquids described by the LJ potential have $\eta(T) > 3$, while the *cold liquids* quoted above reach much lower values, with $\eta(T) \approx 1$ at their triple point.

The size dependence of $\rho(z,L)$ does not fit well in the DF formalism, which provides results for the density profile $\rho(z)$ of infinite flat surfaces, as the density distributions which minimize the grand potential energy $\Omega[\rho(z)] = \mathcal{F}[\rho(z)] - \mu N$. This apparent contradiction comes from the approximate character of $\mathcal{F}[\rho]$, which neglects the CW long-ranged surface correlations [22]. Hence, the liquid-vapor $\rho(z)$ from any DF approximation might be interpreted [23] as an *intrinsic* density profile, including the correlations up to an effective transverse length L_{eff}, assumed to be a few molecular diameters. The extremely weak L dependence of monotonic density profiles makes nearly irrelevant the precise estimation of L_{eff}, and the DF profiles $\rho(z)$ have often been compared with simulation results without explicit reference to L. However, the strong sensitivity of the density layering amplitude to L offers both a problem, for the direct comparison of DF profiles with computer simulations or experimental data, and an opportunity to use it to estimate L_{eff}. To that effect, we built on the concept of a strongly oscillatory *intrinsic profile* with layering amplitudes A_o similar to the bulk liquid density ρ_o, and associated to a transverse sampling size $L_o \approx \sigma$. That concept was strange to the classical view of sharp but monotonic intrinsic profiles, but it was presented first in the analysis of x-ray reflectivity data [5,8,9], and recently checked with MC simulations of cold liquids [21]. Although the use of such short sampling area requires an important reformulation of the classical CW theory [21], we take here a naive view and assume that $A(L) = \rho_o (L_o/L)^{\eta}$, with a free parameter L_o which represents the (extrapolated) sampling length at which the amplitude of the layering becomes equal to the bulk density. In the next section, we present the models and the DF approximations used in this work. In Sec. III, we analyze the results for the density decay modes towards the bulk liquid at coexistence with its vapor. In Sec. IV, we get the density profiles and the surface tension for the free liquid-vapor interfaces, and in Sec. V, we extend the analysis to liquid surfaces in the presence of an external gravitylike field. Finally, a global discussion of all these aspects is presented as a conclusion.

II. MODELS AND DENSITY FUNCTIONAL APPROXIMATIONS

We study several pair interaction models which have been recently developed [7,17] to represent some features of liquids metals with low freezing temperature (Na and Hg). The pairwise potentials are cast into a common functional form,

$$\phi(r) = \phi_0\, e^{-ar} - \phi_1 \sum_{i=1}^{n} e^{-b(r - R_i)^2}, \tag{3}$$

with an exponential repulsive term, controlled by the exponent a and the prefactor ϕ_0, and $n = 1$ or 2 Gaussian wells to represent the attraction, controlled by b, ϕ_1, and the n values of R_i.

Reduced units for these interaction models are defined to mimic those of the LJ system. Thus we define the *molecular diameter* σ such that $\phi(\sigma) = 0$, as the separation between the potential well and the repulsive core. The units of energy are given by the total integral of the potential well in each model,

TABLE I. Parameters in Eq. (3) for the effective pair potentials used in this work. Reduced units σ and U are used.

Parameter	Hg	Na	SA
ϕ_0/U	1.7023×10^{15}	2323.69	199.047
ϕ_1/U	0.62234	0.97529	1.11604
$a\sigma$	35.3789	7.77647	5.10372
$b\sigma^2$	10.6189	2.59724	2.59677
R_1/σ	1.00349	1.01415	1.01463
R_2/σ	1.40132		

$$U = -\frac{9}{8\sigma^3}\int_\sigma^\infty dr\, r^2\, \phi(r), \tag{4}$$

with the prefactors chosen to give precisely $U=\epsilon$ for the LJ model, $\phi_{\rm LJ}(r)=4\epsilon[(\sigma/r)^{12}-(\sigma/r)^6]$.

Despite their common functional form (3), the interaction potentials obtained with the different sets of parameters in Table I, and represented in the inset of Fig. 1, have very distinct characteristics. The Hg model, $\phi_{\rm Hg}(r)$, has a very sharp repulsive core, and a broad and flat potential well, made by the superposition of two Gaussians in Eq. (3). It was developed from a fit to the structure factor of hot liquid mercury, and in previous MC simulation studies it was shown to have a low ratio between the triple point and the critical temperatures, $T_t/T_c\approx0.27$ (to be compared with $T_t/T_c\approx0.56$ for the LJ model), while the FW line crosses the liquid-vapor coexistence at high temperature $T_{\rm FW}/T_c\approx0.88$ (similar to the LJ result). The main characteristics of the Na model, $\phi_{\rm Na}(r)$, obtained from a fit to theoretical results for the energy of expanded crystals, is its soft repulsive core,

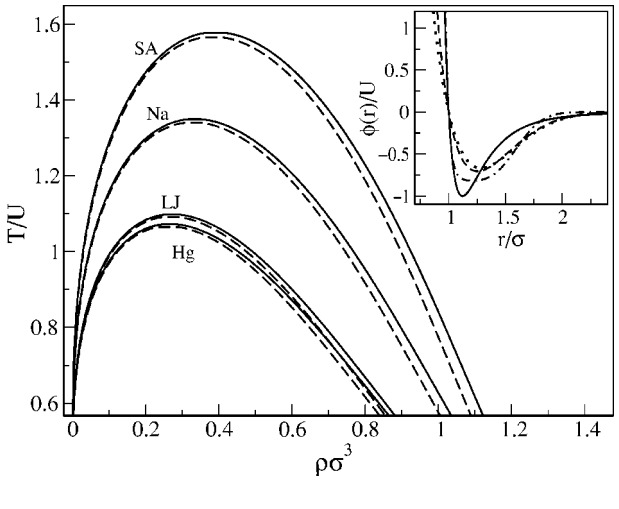

FIG. 1. The liquid-vapor phase diagram for the $\phi_{\rm Na}$, $\phi_{\rm LJ}$, $\phi_{\rm SA}$, and $\phi_{\rm Hg}$ model potentials, obtained using the MF-WDA functional (full line) and the MF-FMT functional (dashed line). Inset shows the effective pair potentials analyzed in this work: full line, Lennard-Jones potential $\phi_{\rm LJ}$; dashed line, alkali-like potential $\phi_{\rm Na}$; dotted line, potential with a softer repulsive part, $\phi_{\rm SA}$; and dotted-dashed line, Hg-like potential, $\phi_{\rm Hg}$. Reduced units σ and U are used.

which is enhanced in the SA (*soft-alkali*) model. These models have low melting temperatures ($T_t/T_c\approx0.22$ for Na and $T_t/T_c\approx0.10$ for SA), but also low FW temperatures ($T_{\rm FW}/T_c\approx0.68$ and $T_{\rm FW}/T_c\approx0.32$, respectively), so that they offer a good set to explore the relevance of $T_{\rm FW}$ for the formation of layering structures at their free liquid surfaces.

We have explored these models with DF approximations based on the separation of the interaction potential, $\phi(r)$, as a core term, $\phi_r(r)$, represented by a hard-sphere fluid; and an *attractive tail*, $\phi_a(r)$, treated in the mean-field (MF) approximation,

$$\mathcal{F}[\rho] = \mathcal{F}_{\rm HS}[\rho] + \frac{1}{2}\int d\mathbf{r}\int d\mathbf{r}'\rho(\mathbf{r})\rho(\mathbf{r}')\phi_a(|\mathbf{r}-\mathbf{r}'|). \tag{5}$$

The decomposition of $\phi(r)$ is done with the simplest method of Baker and Henderson [24], with $\phi_a(r)=\phi(r)$ but restricted to $r\geqslant\sigma$, and the reference HS fluid taken to have a temperature-dependent diameter

$$d_{\rm HS}(T) = \int_0^\sigma dr\left[1-\exp\left(-\frac{\phi(r)}{kT}\right)\right], \tag{6}$$

which is very close to σ for the hard core of the Hg model, and well below σ for the soft core of the SA model. The hard-sphere free-energy density functional $\mathcal{F}_{\rm HS}[\rho]$ is approximated by two different nonlocal approximations; the first is a version [25] of the weighted density approximation (WDA), developed to reproduce the quasiexact Carnahan-Starling equation of state of the HS fluid. The second is a more recent [26] version of the fundamental measure theory (FMT), developed from the concept of dimensional crossover [27] and which reproduces the Percus-Yevick equation of state and direct correlation function, $c(r)$, of the bulk HS fluid.

Density functional approximations like Eq. (5) have been extensively used for the study of wall-fluid and fluid-fluid interfaces, including systems with strong surface layering [6,14,25,26]. When applied to bulk fluids, they give the extended van der Waals approximation, with the free energy per unit volume

$$f(T,\rho) = kT\rho\left[\log(\rho)-1+\Delta\psi_{\rm HS}(\rho)\right] - \frac{16\pi}{9}U\sigma^3\rho^2, \tag{7}$$

where $\Delta\psi_{\rm HS}(\rho)$ is the free energy excess per particle in the HS fluid, with respect to the ideal gas. The liquid-vapor phase diagrams from that free energy (shown in Fig. 1) are very similar for both choices for the HS equation of state, while the extended van der Waals approximation exaggerates the difference between the soft-core repulsion of the Na and SA models, with respect to the harder repulsion of the Hg model; we include for comparison the results with the LJ potential. The results for the critical temperatures (Table II) show deviations, with respect to those obtained by MC simulations [17], which span from a 10% overestimation of T_c for the SA model to a 10% underestimation for the LJ and the Hg models. Away from the critical region, the main drawback of the DF approximation (5) would appear in the study of the crystalline solid phases, since neglecting the effects of

TABLE II. The reduced critical temperature T_c/U and the ratio between the critical and the Fisher-Widom temperatures T_{FW}/T_c, for the different effective pair potentials. The Monte Carlo (MC) results from Ref. [31] are compared with the two DF approximations, MF-WDA and MF-FMT, used in this work.

	T_c/U				T_{FW}/T_c			
	LJ	Hg	Na	SA	LJ	Hg	Na	SA
MC	1.21	1.17	1.25	1.43	0.89	0.88	0.68	0.32
WDA	1.098	1.074	1.349	1.577	0.864	0.871	0.725	0.622
FMT	1.092	1.067	1.340	1.565	0.864	0.871	0.702	0.580

the correlation structure in the liquid destabilizes this phase with respect to the crystalline solid, described within the DF formalism as a strongly self-structured density distribution [28]. There are several proposals to solve this problem [29,30] which have been used with good results for the LJ fluid, but they lead to more cumbersome functional forms. Therefore, we keep Eq. (5) at the minimum level of complexity to get a qualitatively accurate representation of the liquid-vapor phase diagram, of the bulk direct correlation function, and of the liquid surface structure. In all the following, we disregard the solid phase which would be predicted by our DF approximation, as far as the bulk liquid becomes locally stable, with respect to the self-modulation of the density distribution.

III. BULK ASYMPTOTIC DECAY MODES

The generic functional analysis of the decaying density oscillations [6,13] offers a direct way to calculate the exponential decays, associated to the oscillatory and the monotonous modes in Eq. (1), from the roots of the equations

$$1 = 4\pi\rho \int_0^\infty dr\, r^2 c(r) \frac{\sinh(\alpha\, r)}{\alpha\, r} \cos(q\, r) \tag{8}$$

and

$$1 = 4\pi\rho \int_0^\infty dr\, r^2 c(r) \cosh(\alpha\, r) \frac{\sin(q\, r)}{q\, r}, \tag{9}$$

simultaneously solved for the real α and imaginary q parts of the complex decay; and from the solution of Eq. (8), to give $\beta = \alpha$ with $q = 0$, for the real exponential decay.

The direct correlation functions, $c(r)$, in Eq. (9) for the bulk liquids are consistently given within each DF approximation by the second functional derivative of $\mathcal{F}[\rho]$, so that from Eq. (5) we get

$$c(r) = c_{HS}(r) - \beta\phi_a(r), \tag{10}$$

with a density-independent contribution from the attractive interactions $\phi_a(r)$, and a HS contribution which is exactly the result of the Percus-Yevick approximation in the FMT density functional [26] and includes a small tail in $r \geqslant d_{HS}$ for the WDA functional [25].

The results for α, q, and β, obtained from that $c(r)$ and shown in Fig. 2, have the same qualitative trends as those from MC simulations [31]. The imaginary part q of the oscillatory mode has a weak dependence with T, going from values just above $2\pi/\sigma$ at low temperatures to values around $5/\sigma$ near the critical point, for all the models. The real part of the oscillatory mode, $\alpha(T)$, increases with T, while that of the monotonic mode, $\beta(T)$, is always a decreasing function, vanishing at the critical point, as the inverse correlation length. The different DF approximations for the HS free energy have little effect in β, with the WDA results always

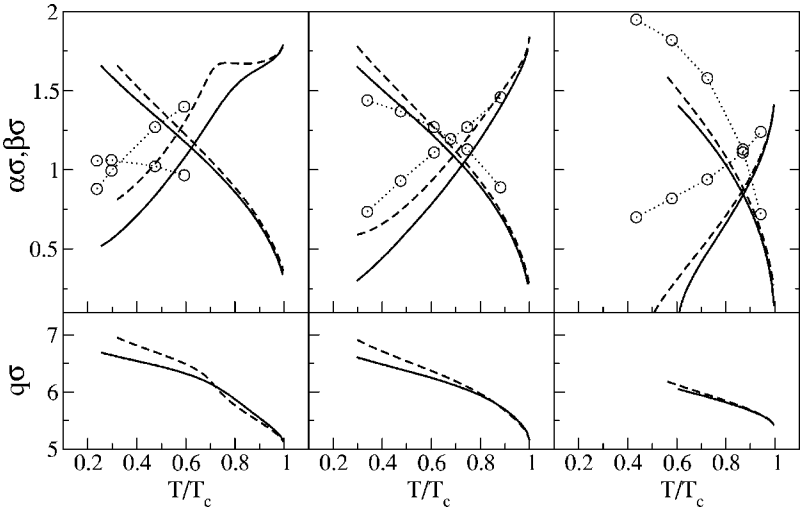

FIG. 2. Exponential decay parameters in molecular diameter units, obtained from Eqs. (8) and (9) for the liquid along the coexistence curve, with the *soft-alkali* (SA), *sodium-like* (Na), and *mercury-like* (Hg) model interactions. The results for the two DF approximations are given by the full lines (MF-WDA) and the broken lines (MF-FMT). In the upper panels, the decreasing curves show the real exponential decays $\beta\sigma$ and the increasing curves the real part of the exponential decays $\alpha\sigma$, with the imaginary part $q\sigma$ in the corresponding lower panel. The symbols and the dotted line (as a guide to the eye) are the results for $\alpha\sigma$ and $\beta\sigma$ obtained with the Monte Carlo simulations in Ref. [31].

slightly below those from the FMT. Compared with the MC results in terms of the respective T/T_c, the DF approximations overestimate β for the SA model and underestimate it for the Hg model, with the Na model in between.

In contrast, the DF results for α are always below the MC data, but now the differences between the two versions for the nonlocal dependence of the HS free energy are more important; the most advanced FMT description reduces by half the difference between the WDA and the MC results for the SA and the Na models. However, the largest difference for α is found in the Hg model, and it is less dependent on the quality of $\mathcal{F}_{\mathrm{HS}}[\rho]$. This is related to the physical differences between the *cold liquids* models; they all share the property of a low ratio T_t/T_c, but they get it from different effects. The soft core repulsion of the Na model, and its exaggerated SA version, produces the stabilization of the liquid with respect to the crystal; this effect is incorporated in the DF approximation by the choice of the effective HS radius at each temperature (6), and the relatively good agreement between the FMT and the MC results for the Na model indicate that this procedure is fairly efficient. The extreme softness of the SA model makes Eq. (6) less accurate, but still there is an important improvement when we shift from the WDA to the FMT treatment of the HS nonlocal density dependence. On the other side, the Hg model has a very sharp core, which should be well represented by $\mathcal{F}_{\mathrm{HS}}[\rho]$, but it gets its low triple point from the strong correlations in the dense liquid, to optimize the occupation of its flat and broad potential well. Such a difference between the correlation structure in the liquid and that of the reference HS fluid is fully missed by our MF approximation (5). The qualitative consequence of that failure is the rapid decrease of the DF results for α which decreasing T, so that at $T/T_c \approx 0.6$ in the WDA, and 0.52 in the FMT, we get $\alpha=0$, and the liquid becomes unstable with respect to a structured (solid) phase.

The FW temperatures, given in Table II, are defined as those where $\alpha(T_{\mathrm{FW}})=\beta(T_{\mathrm{FW}})$, and give the boundary between the monotonous and oscillatory modes as the slower decaying perturbation of the bulk liquid. For the Hg model, the values of T_{FW} with both DF approximations are very close to those obtained with MC simulations [31], but that hides relatively large shifts in the values of $\alpha(T)$ and $\beta(T)$. For the SA model, we get the largest overestimation in the DF value for T_{FW}/T_c, with respect to the MC results, while the good agreement for the Na model reflects that its correlation structure is reasonably described by the HS reference system, without the problems created by the extra-soft core of the SA, or by the non-HS correlations of the Hg model.

IV. LAYERING AT FREE LIQUID SURFACES

The amplitudes A and B for the decaying modes in Eq. (1) are more important than the exponential decays α and β to determine the aspect of the density profiles near the interface. Since those amplitudes cannot be obtained from the linear DF analysis, we have to shift to a numerical minimization of the grand-potential energy $\Omega[\rho]=\mathcal{F}[\rho]+\mu\int d\mathbf{r}\rho(\mathbf{r})$ with respect to planar profiles, $\rho(\mathbf{r})=\rho(z)$, with the boundary values ρ_l and ρ_v, away from the interface. We have used a standard conjugated-gradients method to minimize the surface tension $\gamma=(\Omega[\rho]-\Omega_{bulk})/A$, and to get the equilibrium values and density profile. Therefore, using the values of γ together with α and q from Eqs. (8) and (9), at each temperature and model interaction we may obtain the DF results for the exponent $\eta(T/T_c)$ defined in Eq. (2), which are presented in Fig. 3, and compared with the Monte Carlo results for the same models [17]. That comparison shows a fair agreement between the DF and MC results for η, when represented in terms of the critically scaled temperatures T/T_c; also the results for the different model interactions fall into an approximately common shape, i.e., roughly following a *law of corresponding states*. The rapid increase of η with T/T_c is a consequence of the decrease of γ as we approach the liquid-vapor critical point; therefore the critical divergence of η at $T=T_c$ should certainly have a different shape from the MC simulations and from the mean-field DF calculations, but those bulk critical differences do not show up in the temperature range ($T \leqslant 0.7\ T_c$) explored here.

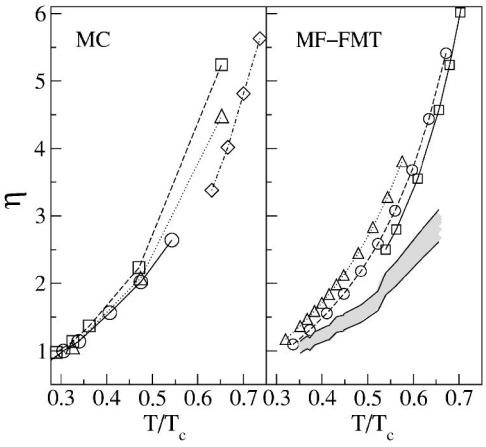

FIG. 3. The capillary wave exponent η for the free liquid surface obtained from Monte Carlo simulations (left panel) using $\eta(T)=kT\pi/\gamma\sigma^2$, and from the MF-FMT approximation (right panel) using $\eta(T)=kT(\alpha^2+q^2)/4\pi\gamma$. Circles: *sodium-like* (Na) potential ϕ_{Na}; triangles: potential with a softer repulsive part, ϕ_{SA}; squares: *mercury-like* (Hg) potential, ϕ_{Hg}; and rhombus: Lennard-Jones potential ϕ_{LJ}. The shadowed band in the right panel gives the estimation for the effective η obtained from the values of $L\eta$ given by Eq. (16), and assuming that $L=12\pm1\sigma$ for all the temperatures and models.

The insets in Fig. 4 present typical density profiles, comparing the results of the two versions for $\mathcal{F}_{\mathrm{HS}}[\rho]$, and the dependence with the temperature (tied to the change in the coexisting bulk densities), while the broad views of the interfaces are shown in detail in the main figures. The oscillations observed for the density profiles at low temperatures are qualitatively similar to those observed for the SA and Hg models in MC simulations [7,16] and also to those obtained for a square-well potential in previous studies with a similar DF approximation [6]. The main difference between the results appears when the WDA is used to describe the HS core in the Hg model, since a vanishing $\alpha(T)$ produces the propagation of the oscillatory structures very deep into the liquid bulk [notice the extended z scale in Fig. 4(c)]. Otherwise, the

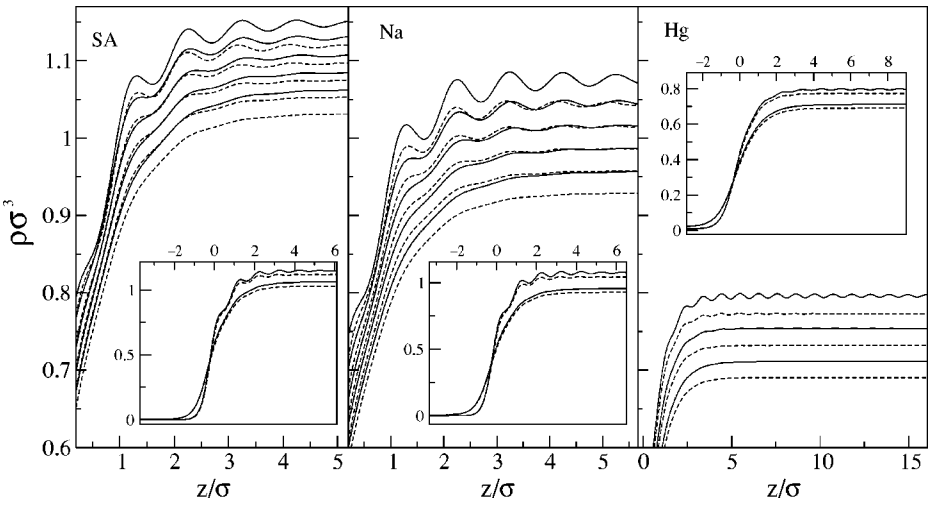

FIG. 4. Liquid-vapor density profiles in reduced units, z/σ and $\rho\sigma^3$, obtained for the three model potentials (SA, Na, and Hg) with the MF-WDA (full line) and the MF-FMT (dashed line) density functional approximations. The different curves, with decreasing bulk densities, correspond to increasing temperatures: $T/U=0.50$, 0.55, 0.60, 0.65, 0.70 for the ϕ_{SA} and ϕ_{Na} models; and $T/U=0.65$, 0.70, 0.75 for the ϕ_{Hg} model. The insets show broad views of the profiles for the upper and lower temperatures in each model.

results are qualitatively similar for all the models and DF approximations, with surface layering becoming weaker as T increases. The numerical accuracy of the DF results allows the observation of density oscillations with tiny amplitudes, which would be well below the intrinsic noise of any computer simulation, and the fits of the decaying tails to the generic form (1) give the values of the complex and real exponential decays, α, q, and β, together with the respective amplitudes A and B, all as functions of T along the coexisting liquid densities for each model. The values have some dependence on the range of z used for the fits, since very close to the interface there are other (faster decaying) terms which would contribute to $\rho(z)-\rho_l$, while too far from the interface the amplitudes are too small, even compared with the small numerical noise from the minimization of $\Omega[\rho]$. Nevertheless, there is a generally good agreement between the values of α, q, and β obtained from the fits to $\rho(z)$ and those predicted by the linear DF analysis and those values obtained from the fit to $\rho(z)$.

A. The layering amplitude and the Fisher-Widom line

The amplitudes of the two decaying modes of $\rho(z)$ towards ρ_l obtained from the fits (1) give $|B|\sim\rho_l$ and much lower values A, which we may identify down to $10^{-3}\rho_l$, with the main uncertainty coming from the range of z used in the fits. The results for A are presented in Fig. 5 in reduced T/T_c scale of temperatures. The differences between the two DF approximations for each model are not important, within the logarithmic scale used for A, so that we keep the discussion in terms of the FMT results. The differences between the models follow the expected trend: the hard core of the Hg model produces stronger density oscillations at a given T/T_c than the ultrasoft core of the SA model; however, the spurious instability, produced by the MF approximation in our DF results, restricts the temperature range for the Hg liquid to $T/T_c>0.53$, and the observed values of A are a factor 10 below those for the SA and Na models at low temperatures. Thus the results for the different models appear to be shifted along the T/T_c axis, and to show a slightly faster than exponential decay of A with T. The vertical arrows in Fig. 5 mark the values of T_{FW}/T_c for each model and DF approximation. Although the relative shift of $\log(A)$ along the T/T_c axis for the three models follows the same order as T_{FW}/T_c, it is clearly much smaller, so that a scaling dependence of A with $(T_{\mathrm{FW}}-T)/T_c$ should be discarded. For the SA model, we are able to measure the value of $A(T)$ up to T_{FW}, while for the Na and Hg models the amplitude goes below the numerical precision limit for T still away from T_{FW}. This is qualitatively similar to the results observed in the MC simulations of the model, although the exact T_{FW}/T_c is much lower than the present mean-field result, and the intrinsic noise of the MC simulation is much higher than numerical precision of our DF treatment. The lack of correlation between $A(T)$ and T_{FW} for different models was presented as evidence against the link between these two aspects. However, it is still true that we are not able to measure $A(T)$ far above T_{FW}, and only for the SA model may we be able to marginally cross that limit. In contrast, the $g(r)$ of the SA liquid shows clear oscillations,

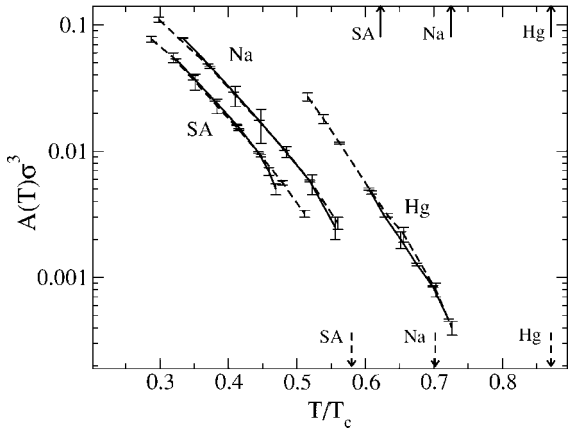

FIG. 5. Amplitude of the oscillatory profiles for the two DF approximations, in reduced units $A\sigma^3$, as defined in Eq. (1) versus the temperature reduced to the critical one, T/T_c, for the ϕ_{Na}, ϕ_{SA}, and ϕ_{Hg} model potentials, using the MF-WDA (full lines) and MF-FMT (dashed lines) DF approximations. The error bars indicate the uncertainty coming from the range of z used in the fits. The vertical arrows (full line upward MF-WDA, and dashed line downward MF-FMT) mark the values of T_{FW}/T_c for each model and DF approximation.

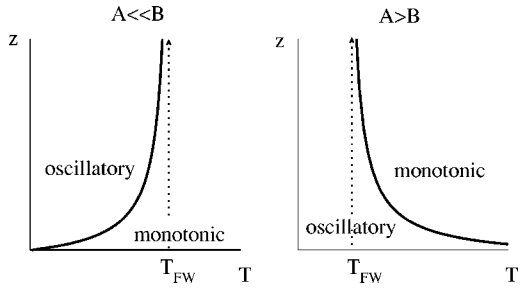

FIG. 6. Sketch of the behavior of the z thresholds that separate the oscillatory from the monotonic part of the profiles. The left figure shows the behavior for $A \ll B$ (as for the liquid-vapor density profiles), and the right figure for $A > B$ [as for a liquid against a wall or the $g(r)$ of the liquid].

leading to easily measurable values of $A(T)$, even at temperatures well above T_{FW}, when the asymptotic decay is monotonic.

An explanation for this behavior may be searched for in terms of the qualitative aspect of $\rho(z)$ created by the superposition of the oscillating and the monotonic modes in Eq. (1). At any $T < T_{\mathrm{FW}}$ [i.e., $\beta(T) > \alpha(T)$], there would be an oscillatory tail, but if the amplitude $A(T)$ for that term is much smaller than the amplitude B for the (faster decaying) monotonic mode, the density profile would become oscillatory only for z above a *lower* threshold

$$z_{\mathrm{min}}^{(\mathrm{osc})}(T) \equiv \frac{1}{\beta - \alpha} \log\left[\frac{B\,\beta}{A\sqrt{q^2+\alpha^2}}\right], \tag{11}$$

which diverges as T approaches T_{FW} from below, as shown in the left sketch of Fig. 6. The fit of the numerical density profiles to the form (1) is in practice restricted to the first 10 or 15 layers, so that near T_{FW} the full range of z would be below $z_{\mathrm{min}}^{(\mathrm{osc})}$ and the qualitative aspect of the liquid-vapor profile would be monotonic. In contrast, for the density profiles of the liquid against a wall, or for the $g(r)$ of the liquid, we expect $A > B$, so that the logarithm in Eq. (11) would be negative and the oscillations would be clear from the first layer at any $T < T_{\mathrm{FW}}$, while above T_{FW} there would still be clear oscillations for z (or r) below an *upper* threshold

$$z_{\mathrm{max}}^{(\mathrm{osc})}(T) \equiv \frac{1}{\alpha - \beta} \log\left[\frac{A\sqrt{q^2+\alpha^2}}{B\,\beta}\right], \tag{12}$$

which diverges as T approaches T_{FW} from above, as in the right sketch of Fig. 6. The qualitatively different aspects of the liquid-vapor density profiles $\rho(z)$ and the pair distributions functions $g(r)$ result from the different values of the term in brackets in Eqs. (11) and (12), with $B \gg A$ in $\rho(z)$ and with $B \ll A$ in $g(r)$, shifting the role of the FW line from Eq. (11) to Eq. (12). Any upper cutoff on z forced by the numerical DF minimization of $\Omega[\rho]$ would reduce the observation of oscillations in the liquid-vapor density profile to temperatures below T_{FW}. Therefore, the relevance of the FW line with respect to the aspect of the density profile, at microscopic distances of the free liquid surface, is not based on the vanishing of $A(T)$, but only in having that amplitude of the oscillatory decay mode, much smaller than the amplitude $B \sim \rho_l$, for the monotonic decay mode in the liquid surface. Systems like those described by the Hg of the Na model interactions have vanishingly small values for $A(T)$ well below T_{FW}, so that the FW line appears to be irrelevant for the aspect of $\rho(z)$. Only because of its low T_{FW} does the SA model show the role of the FW in the aspect of $\rho(z)$, leading to monotonous density profiles within the range of z accessible to our numerical DF calculations, but without a direct effect of T_{FW} on the small amplitude of the oscillatory mode.

B. Capillary waves and the effective DF sampling size

We shift now to analyze the rapid decay of $A(T)$ with increasing temperatures, within the interpretation of $\rho(z)$ as an *intrinsic* profile associated to the sampling of the surface over an effective finite transverse area L_{eff}^2, and hence with a limited role of the capillary waves imposed by the lower wave-vector cutoff $q_l = 2\pi/L_{\mathrm{eff}}$. The direct characterization of the intrinsic surfaces and intrinsic density profiles in Monte Carlo simulations [21] has confirmed the notion, set up in the interpretation of x-ray reflectivity experiments [8], that the intrinsic profiles associated to transverse samplings of $L_o \approx \sigma$ have strong oscillatory structures, with amplitudes A_o similar to the liquid bulk density ρ_l. Within the assumptions of the CWT [15], the amplitude of the oscillations, sampled over a transverse linear size L, goes proportional to $L^{-\eta(T)}$, with the exponent defined in Eq. (2). In order to fix the proportionality constant in that relation, we may arbitrarily choose an amplitude A_o equal to the bulk liquid density ρ_l, and use $A(T) = A_o\,(L_o/L_{\mathrm{eff}})^{\eta(T)}$ in terms of the effective transverse size L_{eff} which is built in a DF approximation, and an intrinsic length scale L_o, which may depend on the model interaction but is expected to have values around σ. Qualitatively, the value of L_o would correspond to transverse sampling sizes so short that there is no room for the CW damping of the oscillatory structure associated to bulk correlation structure in the liquid, with layering amplitude of the same order of the bulk density.

In Fig. 7, we compare the results for $A(T)$ obtained with the FMT-DF, and the functions $\rho_l(T)\,(L_o/L)^{\eta(T)}$, for different values of L/L_o, using the values of ρ_l and η given by the same DF approximation. There is a semiquantitative agreement, in the sense that the fast decay of $A(T)$ over a narrow range of T/T_c is indeed compatible with the CW damping of the density oscillations. However, the decay of $A(T)$ not being as rapid as that of $\rho_l(T)(L_o/L)^{\eta(T)}$ for a fixed L/L_o, so that the most naive assumption $L_o \approx \sigma$ for all the models, would imply the decay of L_{eff} with the temperature. For the SA model, L_{eff}/L_o falls from 14 to 8, for the Na model from approximately 12 to 7, and for the Hg model from 5 to 3. Such variations with temperature should be compared with the bulk correlations lengths β^{-1} and α^{-1}, the first one increasing with T while (below T_{FW}) the second one is larger and decreases with T. Their typical values are β^{-1} from 0.6 to 0.8σ, and α^{-1} from 1.8 to 1.25σ in the SA model, over the same range of T/T_c as used to get $A(T)$; while for the Hg model β^{-1} goes from approximately 0.67 to 1.0σ, and α^{-1} decreases from 3.5 to 1.5σ. Notice that, if we take the naive

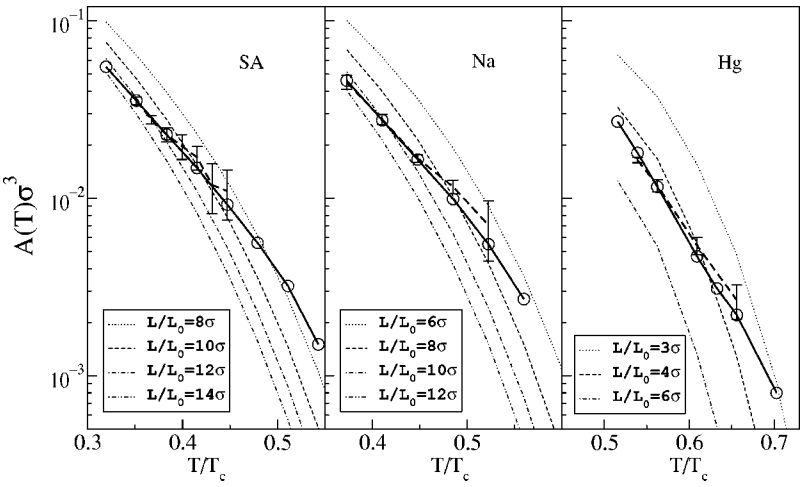

FIG. 7. Amplitude of the oscillatory profiles for the FMT-PY approximation, in reduced units $A\sigma^3$, versus the temperature reduced to the critical one, T/T_c, for the ϕ_{SA} (left panel), ϕ_{Na} (middle panel), and ϕ_{Hg} (right panel) model potentials. The circles and full lines show the same values (but without error bars) as shown in Fig. 5 from the fits to Eq. (1). The thin lines are the functions $\rho_l(T)(L_o/L)^{\eta(T)}$, for different values of L/L_o, with $\eta(T)=kT(\alpha^2+q^2)/4\pi\gamma$. The broad dashed line is the same function but now η is obtained from the estimation for the effective value of $L\eta$ given by Eq. (16) with $L=12\sigma$.

assumption $L_o \approx \sigma$, the tendency with T/T_c within a model would suggest the correlation between L_{eff} and α^{-1}, but the comparison between the models goes against such correlation, and the large difference between the predicted values of L_{eff} for the SA and the Hg models does not correspond to any equivalent change in the properties of their bulk liquids. A more educated guess for L_o should take into account that the sharper core repulsion of the Hg model should produce stronger oscillations, so that the sampling size L_o to get (or extrapolated to) $A=\rho_l$ should be much larger than for the soft-core repulsion of the SA model. That interpretation might account for the differences between the values of L_{eff}/L_o for the different models, but it would leave us short of information to get a quantitative estimate of L_{eff} from $A(T)$, since we cannot discern the value of L_{eff} without accepting its strong dependence with T, and then it would be impossible to separate it from the scale L_o used to transform the proportionality $A \sim L^{-\eta}$ into a quantitative relationship.

V. LIQUID SURFACES IN EXTERNAL FIELDS

In this section, we explore the effect of a gravitylike field to add a new control variable to identify the effective length L_{eff}. In the presence a uniform external field, mg, acting on the particles of the fluid along the z direction, the CW damping of the density oscillations goes like

$$\frac{A(T,mg)}{A_o} \approx \left[\left(\frac{L_o}{L}\right)^2 + \frac{(\rho_l-\rho_v)mg}{(2\pi)^2\gamma}\right]^{\eta/2}, \tag{13}$$

and it becomes independent of L when this transverse size goes well below the *capillary length* $\xi_{\mathrm{cap}}=[(\rho_l-\rho_v)mg/\gamma]^{-1/2}$.

The typical effect of the Earth gravity field on a liquid surface (with ξ_{cap} in the range of millimeters) would be fully irrelevant for any system with L in the range of a few molecular diameters. Thus to get an appreciable effect of g on the density profiles from our DF treatment, we should include much stronger external fields, which would have a non-negligible effect on the density of the liquid bulk, creating a continuous variation of $\rho(z)$, instead of a flat asymptotic profile. In order to reduce this effect, we have used the external potential

$$V_{\mathrm{ext}}(z) = -mg\lambda \tanh\left(\frac{z}{\lambda}\right), \tag{14}$$

to be nearly linear for $|z|<\lambda \equiv 18.33\sigma$, and to go nearly flat at the extreme of our functional minimization box, which we take at $z=180\sigma$. $V_{\mathrm{ext}}(z)$ provides a nearly uniform force mg acting on the molecules in the interfacial region, but smoothly vanishing in the two bulk phases, to avoid the spurious interference with any oscillatory structure created at the borders of our variational space. The density profiles in Fig. 8 show that a gravity field $\beta mg\sigma=0.01$ (about 10^{12} times the Earth gravity) produces very little changes in the aspect of $\rho(z)$ around the interface. Increasing the field by one order of magnitude produces some changes in the oscillatory structure of $\rho(z)$, but superimposed on a continuous increase of the liquid density, which has to be extracted before using a fit similar to Eq. (1). This is done by means of the local density profile $\rho_{\mathrm{LD}}(z)$, which solves the equation

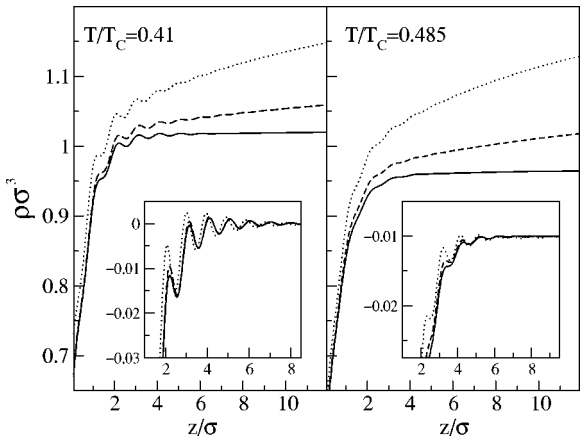

FIG. 8. Liquid-vapor density profiles in the presence of a gravity field in reduced units, z/σ and $\rho^*=\rho\sigma^3$ obtained for the ϕ_{Na} interaction with the MF-FMT density functional approximation. The continuous lines are for an external field of $\beta mg\sigma=0.01$; the dashed line: 0.1; and the dotted lines: 0.4; the left panel corresponds to $T/T_c=0.410$ and the right one to $T/T_c=0.485$. The insets show $\rho(z)-\rho_{\mathrm{LD}}(z)$, to be used in the fits for the layering amplitude.

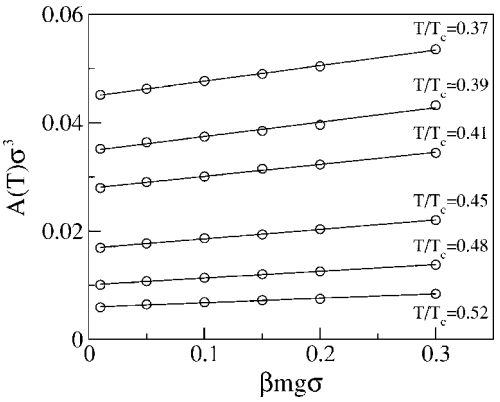

FIG. 9. Amplitude of the FMT-PY oscillatory profiles for the ϕ_{Na} model potential at several temperatures, as a function of gravity field $\beta mg\sigma$. The lines are the linear fits corresponding to Eq. (15).

$$\mu_o(T) = \mu(T, \rho_{\mathrm{LD}}(z)) + V_{\mathrm{ext}}(z),$$

where $\mu(T,\rho) \equiv \partial f(T,\rho)/\partial\rho$ is the chemical potential as a function of the density, from the bulk free energy (7), and $\mu_o(T)$ is the chemical potential at liquid-vapor coexistence. The insets in Fig. 8 present the difference $\rho(z) - \rho_{\mathrm{LD}}(z)$, which may now be fitted to the form (1) to extract the amplitude $A(T,mg)$ for the surface layering.

In Fig. 9, we present the layering amplitude for the Na model, at several temperatures, as a function of $\beta mg\sigma$. Restringing ourselves to a small range of external fields, strong enough to make a difference between $A(L,mg)$ and $A(L,0)$, but weak enough to make valid the LDA representation of the monotonic increase in $\rho(z)$, we may only discern the linear term in a Taylor expansion of Eq. (13),

$$\frac{A(T,mg)}{A_o} \approx \left(\frac{L_o}{L}\right)^{\eta}\left[1 + \frac{(\rho_l - \rho_v)mgL^2\eta^2}{2\pi(q^2+\alpha^2)} + \cdots\right], \quad (15)$$

at first order in mg, and where we have used Eq. (2) to express the surface tension in terms of η.

The relative increase of $A(T,mg)$ with mg, from the zero field value $A(T,0)$, gives a direct estimation for the effective value of $L\eta$,

$$L\eta|_{\mathrm{eff}} = \left[2\pi(q^2+\alpha^2)kT\frac{A(T,g) - A(T,0)}{mgA(T,0)}\right]^{1/2}. \quad (16)$$

This expression is independent of A_o and L_o, and our results in Fig. 10, for the effective value of $L\eta$, follow quite well a *law of corresponding states* similar to that observed for $\eta(T/T_c)$ in Fig. 3.

The most direct way to get the effective sampling size L_{eff} would be from the ratio between Eqs. (16) and (2). The results, in the Fig. 10 inset, are independent of the unknown value of L_o at which the amplitude is assumed to go to $A = \rho_l$, and which should depend on the atomic interaction model. Now, we may use these L_{eff}, together with the amplitudes A in Fig. 7 and the exponent η in Fig. 3, to estimate $L_o = L_{\mathrm{eff}}(A/\rho_l)^{1/\eta} \approx 0.8\sigma$ for the SA, $L_o \approx 1.05\sigma$ for the SA, and $L_o \approx 2\sigma$ for the Hg model, which correlate well with the sharpness of their core repulsions. Nevertheless, those results

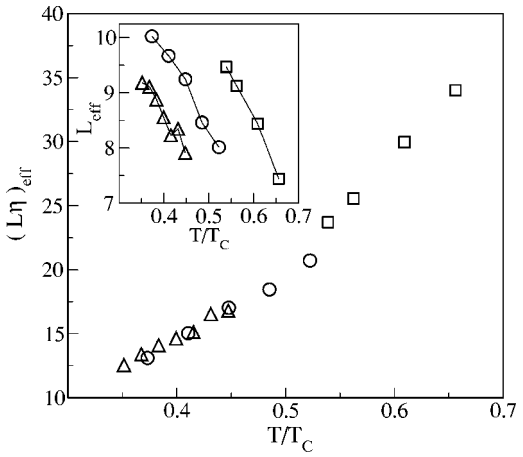

FIG. 10. The effective value of ηL_{eff} for the three model potentials: SA (triangles), Na (circles), and Hg (squares), obtained from Eq. (16) with the MF-FMT density functional. The inset shows the inferred values of the effective DF sampling length L_{eff}, from the ratio between ηL_{eff} and the values of η obtained from the surface tension in Eq. (2). The lines are guides to the eyes.

for L_{eff} still show a rapid decay with the temperature, which, away from the narrow range of temperatures in which we are able to keep track of the density oscillations, would extrapolate to unrealistically low values of L_{eff} at high T. Also, it seems strange that, within this interpretation, the fairly accurate law of corresponding states observed for $L\eta$ from Eq. (16) would come from a cancellation between the stronger model dependences of η and L_{eff}. An alternative view is that we may have an approximately constant and common value, $L_{\mathrm{eff}}/\sigma \approx 10 \pm 2$ for all the models, which would lead to a fair agreement between the results of Eqs. (2) and (16) at low temperature, but which would imply (as shown in Fig. 3) an important reduction in the effective values of η which describes the effects of the CW damping at the higher T. Such internal inconsistency is typical of DF approximations, which give different results for the correlations evaluated as a direct response to an externally imposed density change [like in the test particle route to get $g(r)$], and when they are evaluated through the internal DF relationships for the unperturbed system [i.e., like the Orstein-Zernike approach to $g(r)$ from $c(r)$]. In our case, the free-energy cost of an externally imposed CW-like modulation of the surface may be well estimated by the DF approximations, as reflected in the good values obtained for $\eta(T/T_c)$; however, the role of such long-ranged surface correlations is not built in the same DF approximations, so that they underestimate their effects in the damping of the layering structures, and hence the value of $\eta(T/T_c)$ estimated from Eq. (16). With the estimate of a constant $L_{\mathrm{eff}} \approx 12\sigma$ and the values of $\eta(T/T_c)$ obtained from Eq. (16), the results in Figs. 5 and 7 would be compatible with values of L_o slightly shorter than those quoted above, but still in qualitative agreement with the expected differences created by the sharp core of the Hg model versus the soft and ultrasoft repulsions of the Na and the SA models.

VI. CONCLUSIONS

We have analyzed in detail the layering structures predicted by DF approximations applied to the liquid-vapor in-

terfaces of fluids with low triple-point temperature, which were developed and used to confirm the existence of such oscillations in MC simulations [7,17]. The DF results for the phase diagrams, the exponential decays of the density perturbations, the FW temperature at coexistence, and the amplitude of the layering structures are in qualitative agreement with our previous MC simulation results for the same model interactions, although there are important quantitative differences, as expected from the simplified DF treatment of the strong correlations in such *cold liquids*.

The high precision of the DF minimization allows us to extract the amplitudes A and B for the oscillatory and the monotonic density decay modes much more accurately than the limit imposed by the intrinsic noise in MC simulations. Altogether, the DF results for $A(T)$ support the same conclusions as those from MC simulations; the amplitude $A(T)$ decays rapidly with increasing temperature, but without visible correlation with $T_{\mathrm{FW}}-T$ terms of the FW temperature for each model. Nevertheless, we give a generic argument (sketched in Fig. 6) for the absence of oscillations when the system approaches T_{FW} with a nonvanishing but small-amplitude $A(T)$. The apparently different aspect of the liquid vapor density profiles and those for the liquid against a hard wall or the bulk liquid $g(r)$ at temperatures around T_{FW} would be explained by the relative amplitudes of the monotonic and the oscillatory modes for the density perturbations, which shift the relevance of the FW line from Eq. (11) to Eq. (12). Hence we may conclude that T_{FW} is not of relevance for the temperature dependence of $A(T)$, but it still sets the threshold for the relevance of a small amplitude on the *aspect* of the density profiles $\rho(z)$.

The alternative explanation for the rapid decay of A with T was based on the role of the capillary waves to smooth down the strong oscillations in the *intrinsic* density profiles, associated to samplings of the liquid surfaces over very small transverse sizes, comparable to the molecular diameter σ. This concept, which was first presented in the analysis of experimental x-ray reflectivity results [8,9], has been explored in detail with MC simulations for the same models used here [21]. The prediction within the framework of the CWT is that the amplitude of the density oscillations is exponentially sensitive to the lower cutoff on the CW wave vectors, imposed by the transverse linear size L [15]. Hence, the density profiles of free liquid surfaces, in the absence of any external potential, should be considered as $\rho(z,L)$, i.e., with a direct dependence on L, which does not fit into the DF scheme of $\rho(z)$ obtained from the minimization of $\Omega[\rho]$ for a flat infinite surface. The interpretation [22,23] that the DF profiles should be considered as *intrinsic* profiles associated to an effective L_{eff} set by the lack of long-range surface correlations in the approximations for $\mathcal{F}[\rho]$ leads to the question of how to calibrate that effective transverse size. The strong sensibility of $A(T)$ to the value of L, compared with the weak (logarithmic) dependence of the interfacial width for monotonic profiles, opens the way to a quantitative estimation of L_{eff} from our DF profiles. The good accuracy of our DF estimations for the exponent η in Eq. (2), compared with the MC results in terms of T reduced to the corresponding critical values, gives support to the attempt to get such estimations of L_{eff}.

However, the direct comparison of $A(T)$ with $A_o(L/L_o)^{-\eta(T)}$, in terms of an arbitrary intrinsic amplitude (which we take as ρ_l) which would be observed for (or extrapolated to) a sampling size $L_o \approx \sigma$, implies a strong dependence of L_{eff}/L_o with the temperature and with the model interaction, which is difficult to accept. We searched for the complementary information given by the dependence of the amplitude A on the strength of a gravitylike external field, which competes with L to set the low-wavelength cutoff for the CW damping effects. Within the constrains of external fields strong enough to have a relevant effect, but weak enough not to break down the linear DF analysis leading to Eq. (1), we are able to get an estimate for the effective value of $L\eta$, which fortunately does not depend on the values of A_o or L_o. The results for the effective values of ηL in different models fall nicely within a law of corresponding states, with a common shape when represented in terms of T/T_c, which, together with the equivalent law observed for the direct estimation of η, goes against the strong model dependence of L_{eff} suggested by the analysis of $A(T/T_c)$ at zero field. The direct results for L_{eff} obtained from the ratio between the value of $L\sigma$ extracted from the layering amplitude in external fields, and the direct result for η (2) from the DF results for the surface tension and the exponential decays, lead to values of L_{eff} between 8 and 10σ for the three models, but still with a too rapid decay with T. An alternative explanation may be given in terms of a slightly larger value of $L_{\mathrm{eff}}=12\pm2\sigma$, approximately constants with T and common to all the model interactions, but interpreting that the CW damping observed in the DF results depends on an effective exponent η_{eff}, rather than its value (2), calculated consistently within the DF approximation. The values of η_{eff} within the broadband shown in Fig. 3 are close to those from Eq. (2) at low T, but they fail to follow their rapid increase associated to the decaying values of the surface tension with increasing temperatures and the consequent enhancement of the CW fluctuations. Such inconsistency between the values of η extracted from the DF results and those which are assumed to be built into the correlation structure of the free-energy density functional are typical of any mean-field approximation.

Altogether, we may conclude that the interpretation of the DF profiles for liquid surfaces *as intrinsic* profiles associated to a finite transverse sampling of the interface is consistent with values of $L_{\mathrm{eff}}\approx 10\pm2\sigma$, curiously close to the typical transverse size of the computer simulation boxes which provide the most usual test of the DF results. However, to make that estimate roughly independent of the temperature and the model interaction, we have to accept also an effective exponent η_{eff}, or equivalently an effective surface tension to represent the (reduced) effects of the CW fluctuations included in the DF approximation up to that transverse sampling size. Therefore, the Gaussian convolution of the profile $\rho(z)$ given by a DF approximation, to include the wavelengths $2\pi/L \leqslant q < 2\pi/L_{\mathrm{eff}}$ as predicted by the CWT, could only be taken as a semiquantitative prediction for the L dependence of the actual density profile $\rho(z,L)$ sampled over a large transverse area, like in an x-ray reflectometry experiment. The difference between the direct value of η, from Eq. (2), and its effective value η_{eff} grows with T/T_c, so that in the tempera-

ture range for typical simple fluids, $T \geqslant T_t \approx 0.6T_c$, there would be a very important difference between the actual role of the CW fluctuations in systems with transverse lengths $L \approx 10\sigma$ and those built in a DF approximation with similar values of L_{eff}. That discrepancy should be reduced at the low temperatures accessible to the *cold liquid* models explored here, but then we have to be aware of the strong correlations in these systems, which are left out of the usual DF approximations, and which may frustrate the quantitative accuracy of the results.

ACKNOWLEDGMENT

This work was supported by the Dirección General de Investigación (MCyT) of Spain under Grant No. BFM2001-1679-C03.

[1] R. Evans, in *Fundamentals of Inhomogeneous Fluids*, edited by D. Henderson (Dekker, New York, 1992), p. 3; S. Dietrich, in *Phase Transitions and Critical Phenomena*, edited by C. Domb and J. L. Lebowitz (Academic, London, 1988), p. 1; H. Lowën J. Phys.: Condens. Matter **14**, 11897 (2002), and references therein.
[2] R. Evans, Adv. Phys. **28**, 143 (1979).
[3] C. A. Croxton, *Statistical Mechanics of the Liquid Surface* (Wiley, New York, 1981)
[4] C. A. Croxton and R. P. Ferrier, J. Phys. C **4**, 1909 (1971); Thomas R. Osborn and C. A. Croxton, Mol. Phys. **40**, 1489 (1980).
[5] P. S. Pershan, Colloids Surf., A **171**, 149 (2000); Jeffrey Penfold, Rep. Prog. Phys. **64**, 777 (2001).
[6] R. Evans, J. R. Henderson, D. C. Hoyle, A. O. Parry, and Z. A. Sabeur, Mol. Phys. **80**, 755 (1993).
[7] E. Chacón, M. Reinaldo-Falagán, E. Velasco, and P. Tarazona, Phys. Rev. Lett. **87**, 166101 (2001).
[8] O. Magnussen, B. M. Ocko, M. J. Regan, K. Penanen, P. S. Pershan, and M. Deutsch, Phys. Rev. Lett. **74**, 4444 (1995); E. DiMasi, H. Tostmann, B. M. Ocko, P. S. Pershan, and M. Deutsch, Phys. Rev. B **58**, R13419 (1998).
[9] M. Regan, E. H. Kawamoto, S. Lee, P. S. Pershan, N. Maskil, M. Deutsch, O. M. Magnussen, B. M. Ocko, and L. E. Berman, Phys. Rev. Lett. **75**, 2498 (1995).
[10] O. Shpyrko, P. Huber, A. Grigoriev, P. Pershan, B. Ocko, H. Tostmann, and M. Deutsch, Phys. Rev. B **67**, 115405 (2003).
[11] M. E. Fisher and B. Widom, J. Chem. Phys. **50**, 3756 (1969).
[12] C. Vega, L. F. Rull, and S. Lago, Phys. Rev. E **51**, 3146 (1995).
[13] M. Dijkstra and R. Evans, J. Chem. Phys. **112**, 1449 (2000).
[14] A. J. Archer and R. Evans, Phys. Rev. E **64**, 041501 (2001); J. M. Brader, R. Evans, M. Schmidt, and H. Lowën, J. Phys.: Condens. Matter **14**, L1 (2002).
[15] R. Evans, in *Les Houches, Session XLVIII, Liquids at Interfaces* (Elsevier, New York, 1989).
[16] P. Tarazona, E. Chacón, M. Reinaldo-Falagan, and E. Velasco, J. Chem. Phys. **117**, 3941 (2002).
[17] E. Velasco, P. Tarazona, M. Reinaldo-Falagan, and E. Chacón, J. Chem. Phys. **117**, 10777 (2002).
[18] F. P. Buff, R. A. Lovett, and F. H. Stinger, Phys. Rev. Lett. **15**, 621 (1965).
[19] J. S. Rowlinson and B. Widom, *Molecular Theory of Capillarity* (Clarendon, Oxford, 1982).
[20] S. Toxvaerd and J. Stecki, J. Chem. Phys. **102**, 7163 (1995).
[21] E. Chacón and P. Tarazona, Phys. Rev. Lett. **91**, 166103 (2003); P. Tarazona and E. Chacón, Phys. Rev. B (to be published).
[22] S. Dietrich, J. Phys.: Condens. Matter **8**, 9127 (1996).
[23] K. R. Mecke and S. Dietrich, Phys. Rev. E **59**, 6766 (1999), and references therein.
[24] J. A. Barker and D. Henderson, J. Chem. Phys. **47**, 4714 (1967).
[25] P. Tarazona Phys. Rev. A **31**, 2672 (1985); P. Tarazona, U. Marini Bettolo Marconi, and R. Evans, Mol. Phys. **60**, 573 (1987).
[26] P. Tarazona, Phys. Rev. Lett. **84**, 694 (2000); Physica A **306**, 243 (2002).
[27] P. Tarazona and Y. Rosenfeld, Phys. Rev. E **55**, R4873 (1997).
[28] P. Tarazona, Mol. Phys. **52**, 81 (1994).
[29] W. A. Curtin and N. W. Ashcroft, Phys. Rev. Lett. **56**, 2775 (1986).
[30] L. Mederos, G. Navascués, P. Tarazona, and E. Chacón, Phys. Rev. E **47**, 4284 (1993).
[31] P. Tarazona, E. Chacón, and E. Velasco, Mol. Phys. **101**, 1595 (2003).